Hillslopes in Headwaters of Qinghai-Tibetan Plateau as Hotspots for Dissolved Organic Carbon Processing during Permafrost Thaw

Yuqin Sun[1,2,3], Kale Clauson[4], Min Zhou[1], Ziyong Sun[5], Chunmiao Zheng[2,3] and Yan Zheng[2,3*]

[1] College of Engineering, Peking University, Beijing, 100871, China.

[2] State Environmental Protection Key Laboratory of Integrated Surface Water-Groundwater Pollution Control, School of Environmental Science and Engineering, Southern University of Science and Technology, Shenzhen, 518055, China.

[3] Guangdong Provincial Key Laboratory of Soil and Groundwater Pollution Control, School of Environmental Science and Engineering, Southern University of Science and Technology, Shenzhen, 518055, China.

[4] School of Earth and Environmental Sciences, Queens College, City University of New York, Flushing, NY 11367, USA.

[5] School of Environmental Studies, China University of Geosciences, Wuhan, 430074, China.

Corresponding author: Yan Zheng (yan.zheng@sustech.edu.cn) ORCID 0000-0001-5256-9395

Key Points

- Protein-like fluorophores in dissolved organic carbon (DOC) from permafrost thaw is prevalent in headwaters of Qinghai-Tibetan Plateau.
- New constraint is placed on hillslope groundwater mean transit time (~7 to 25 days) from the DOC loss (ΔDOC) and the decay kinetics.
- Hillslopes in headwaters of QTP are hotspots for subsurface DOC processing before it reaches the main river during seasonal thaw.

Abstract

Climate warming has accelerated thawing of frozen soil in the northern permafrost, supplying dissolved organic carbon (DOC) to streams and rivers with uncertain fate. Although recent incubation experiments have established that permafrost derived DOC is labile, field evidence is rare and ambiguous, with the linkage to surface – groundwater interaction poorly illustrated. Here, we quantify and characterize DOC for eight types of water sampled from a small (25km^2), alpine (elevation 2960 to 4820 m a.s.l) watershed with variably degraded permafrost in the Qinghai-Tibetan Plateau (QTP) in July and September of 2012, 2013 and 2018. Spatially variable dissolved organic carbon (DOC) concentrations with high percentages of protein-like fluorophores (48± 41%, n=91), attributable to frozen soil based on tracers, are detected throughout the watershed. Increasing ΔDOC (loss of DOC) in subsurface waters corresponds to decreasing proportion of protein-like fluorophores and $SUVA_{254}$. Assuming microbial processing of subsurface DOC and using previously established DOC biodegradation kinetics, the mean transit time of groundwater is estimated to be ~ 7 and 25 days based on changes in ΔDOC of 32% and 74% for July and September, respectively. In addition to providing field evidence for prevalence of labile DOC derived from permafrost in surface and subsurface waters of the QTP, the study establishes that very young groundwater participates in alpine hillslope hydrological and biogeochemical processes. Mass balance of DOC input and export fluxes shows a loss of nearly half of the carbon, indicating that hillslopes are hotspots for DOC processing, with subsurface environment playing a key role.

Plain Language Summary

Climate warming leads to massive thaws of the northern permafrost that has increased the release of organic carbon, previously regarded as "stable", into streams and rivers. Recent laboratory studies of Artic permafrost show the rapid biodegradation of permafrost-derived organic carbon, but is it true? For this, we turn to a small, alpine watershed in the Qinghai-Tibetan Plateau with a gradient of permafrost degradation. First, we provide rare field evidence for widespread labile organic carbon in a variety of water types relying on its optical properties. Second, we use stable isotopes and electrical conductivity as "conservative" tracers to compare with dissolved organic carbon that are "reactive" to estimate the loss of organic carbon from its upgradient source to the downslope sampling location. The extent of the loss of DOC in subsurface environment is dependent on the travel time of the groundwater along the hillslope. The labile DOC originating from permafrost soil is quickly dispersed in the watershed, shedding light on previously poorly constrained surface water – groundwater interaction in such settings. Finally, a mass budget finds a large loss of organic carbon within the watershed. Therefore, hillslopes act as hotspots for permafrost-derived organic carbon processing.

Keywords

Qinghai-Tibetan Plateau, Dissolved organic carbon, Permafrost, Alpine watershed, Groundwater transit time, Fluorescence spectroscopy

1 Introduction

Northern permafrost, including 42% of the areal extent of Qinghai-Tibetan Plateau (QTP), is estimated to account for >20% of total global soil organic carbon (SOC) pool of 1832 Pg [*Mu et al.*, 2015; *Tarnocai et al.*, 2009]. The accelerated thawing and degradation in recent decades [*Hinkel and Nelson*, 2003; *Yang et al.*, 2010] has led to the debate on whether the permafrost act as a sink or a source of carbon to the atmosphere [*McGuire et al.*, 2018], with a recent simulation suggesting that abrupt thaw, especially active hillslope erosional features, contributes significantly to carbon losses [*Turetsky et al.*, 2020]. Further, thawed permafrost SOC enters pore water as dissolved organic carbon (DOC), some of which are exported into aquatic system to become components of in-stream carbon cycling. A recent compilation of DOC losses during passage through terrestrial sources to sea has highlighted that freshwaters are hotspots of DOC respiration [*Catalan et al.*, 2016]. In the Arctic region, the net exchange of CO_2 from terrestrial ecosystems is between 300×10^9 – 600×10^9 kg C/yr, and the CO_2 evasion from inland waters are between 40×10^9 – 84×10^9 kg C/yr [*McGuire et al.*, 2009]. The degradation of terrestrial-sourced DOM has contributed substantially to CO_2 released from rivers and lakes [*Kling et al.*, 1991; *McGuire et al.*, 2009]. However, the in-stream DOC processing in Arctic permafrost region has long been masked due to largely recalcitrant nature of DOC inferred from its modern terrestrial source, established primarily from large (14,000 to 855,000 km^2) basin scale studies [*Balcarczyk et al.*, 2009; *Guo and Macdonald*, 2006; *Guo et al.*, 2007; *Kawahigashi et al.*, 2004]. Such recalcitrant characteristics are nevertheless consistent with the existing knowledge of surface water and groundwater interaction with a long retention time in a lateral flow path dominant Arctic permafrost [*Mann et al.*, 2015].

Yet evidence is emerging that some DOC derived from Arctic permafrost is labile and is more complex than previously thought. Incubation experiments of stream DOC supplied by thawed ancient permafrost [*Drake et al.*, 2015; *Drake et al.*, 2018; *Feng et al.*, 2013; *Vonk et al.*, 2015] have identified pronounced losses of "old" carbon, ranging from one third [*Vonk et al.*, 2013] to one half [*Mann et al.*, 2015; *Spencer et al.*, 2015] for DOC with radiocarbon ages of > 10,000 years. Such "old" DOC is exported as baseflow in 6 Arctic watersheds, attributed to deepening of groundwater flow path due to warming [*Barnes et al.*, 2018]. To reconcile with prior findings that DOC in major rivers in the Artic region are primarily modern in radiocarbon ages [*Aiken et al.*, 2014] with low biodegradability [*Mann et al.*, 2015; *Spencer et al.*, 2015], and are terrestrial soil-plant sourced with high aromaticity [*Guo et al.*, 2007; *Guo et al.*, 2010; *Neff et al.*, 2006; *Spencer et al.*, 2008], it has been proposed that respiration of labile but ancient DOC from permafrost thaw occurs in the smaller, headwater watersheds [*Drake et al.*, 2015], acting as a carbon source to the atmosphere.

QTP is of interest not only because its permafrost is the most extensive at the mid- and low- latitude, but also because the spatially heterogenous degradation of permafrost following the topographical variation also influences hydrology [*Cheng and Wu*, 2007; *Yang et al.*, 2010]. Increasing precipitation and glacier melting have led to an expansion of water storage (12.1 ± 0.6 Gt yr^{-1}) [*Yi et al.*, 2016], especially that of groundwater storage (5.01 ± 1.59 Gt yr^{-1}) since 2003 [*Zhang et al.*, 2017]. Given such significant changes in QTP's hydrological cycle, it is likely that groundwater flow is affected [*Ge et al.*, 2011; *Yao et al.*, 2017], yet few studies have examined such multifaceted changes and its biogeochemical implications. Not only conducting field studies in headwaters of QTP is challenging, complex hillslope hydrological processes in headwaters of QTP need to be understood to illuminate the fate of DOC associated

115 with permafrost thaw. Recent but still rare attempts to quantify groundwater mean transit time
116 (MTT), defined as the time that water parcels spend between the time entering the unsaturated
117 zone and the time flowing out of the aquifer [*Benettin et al.*, 2015; *McDonnell et al.*, 2010], have
118 found that the MTT can range from days to weeks, challenging the long-held view of the
119 distribution of transit time ranging from years to decades. Hydrogeological studies of Hulugou
120 watershed (HLGW) have shown that the subsurface water's radiocarbon age is modern and
121 contains ^{3}H at shallow depth (<20 m) in permafrost and seasonal frost zones of the Hulugou
122 watershed of the QTP [Ma et al., 2017], but groundwater MTT has never been assessed in QTP
123 headwaters. Further, how groundwater – surface water interaction in hillslopes of headwater
124 regions of QTP influences the fate of SOC derived DOC through regulating groundwater transit
125 time, and in turn, the carbon loss in headwaters, remains largely unexplored.

126 To illuminate the emerging and likely significant role that hillslope hydrological
127 processes play in biogeochemistry, this study seeks to provide field evidence for labile DOC
128 derived from frozen soil thaw in a small (25 km^2), alpine (elevation 2960 to 4820 m a.s.l)
129 watershed named Hulugou (HLGW) located in the northeastern QTP (Fig. 1). The spatial and
130 temporal variations in dissolved organic matter (DOM) signatures are interpreted to indicate
131 rapid and variable transit time in part caused by changes in groundwater flow paths in response
132 to the freeze-thaw cycle. Finally, how the new constraints on rapid groundwater transit time in
133 the alpine watersheds of the QTP sets the stage for DOC derived from thawing permafrost to not
134 only disperse but also to persist in the headwaters and its implications for the headwaters acting
135 as DOC processing hotspots are discussed.
136

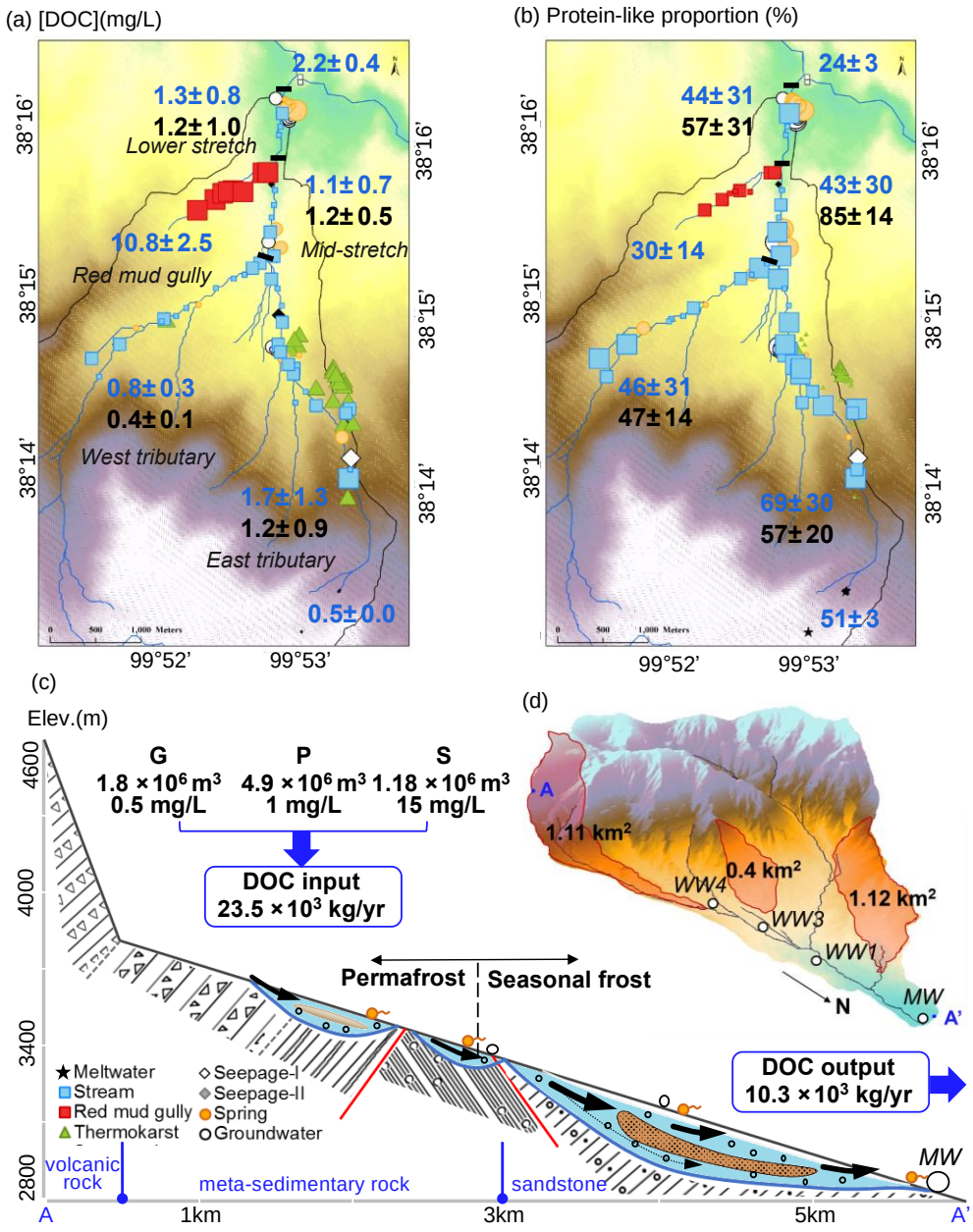

Figure 1. (a) Concentrations of DOC in eight types of water in HLGW, Qinghai-Tibetan Plateau, with legends in panel c. Small, medium and large symbol sizes indicate low (<1.6 mg L^{-1}), medium (1.6-9 mg L^{-1}) and high (>9 mg L^{-1}) [DOC] according to its tertile values. Numbers are mean value ± one standard deviation for [DOC] in stream (blue) and subsurface water (black). **(b)** Proportion of protein-like component identified by PARAFAC modeling, with small, medium and large symbol sizes indicating low (<27.4%), medium (27.4–62.4%) and high (>62.4%) proportions according to tertile values. Numbers are mean value ± one standard deviation for the proportion of protein-like compound in stream (blue) and subsurface water (black). **(c)** A schematic diagram of hillslope hydrological process in HLGW for the cross-section A-A' (inset d, three areas of permafrost and seasonal frost in HLGW are shown, with monitoring wells marked in white circles). Water fluxes and [DOC] in three end members (G: glacier-snow melt, P: precipitation, S: frozen soil meltwater) contributing to DOC input are shown.

2 Material and Methods

2.1 Study Area and Sample Collection

The study was conducted in Hulugou watershed (HLGW), upper Heihe basin, NE Qinghai-Tibetan Plateau (99°50′ – 99°54′ E, 38°12' – 38°17' N; 2960 to 4820 m a.s.l, 25 km^2). The HLGW consists of three geomorphic units of glacier-snow covered mountain, rocky hills, and meadow steppe. Glacier, permafrost and seasonal frost ground have experienced degradation, albeit to different extent within the HLGW [*Li et al.*, 2014]. A first-order stream network with extensive surface water and groundwater exchanges [*Chang et al.*, 2018; *Evans et al.*, 2015] is superimposed on permafrost (3400 m to 4500 m a.s.l) with abundant thermokarst ponds, seasonal frost ground (2900 m to 3400 m a.s.l), and degraded permafrost (3450 m to 3600 m a.s.l) with erosional channels (Fig. 1).

Water samples (n=118) were collected from HLGW for a total of four times in July 2012 (n=22), July (n=28) and September 2013 (n=30), and September 2018 (n=38), respectively. Eleven samples were collected in April 2013 but not discussed in this study. All data from 129 water samples from 5 sampling events are in datasets of Supporting Information.

Eight types of water were sampled, including glacier-snow melt (n=1), streams (n=41), a thermo-erosional red mud gully (n=10), thermokarst ponds (n=27), seepage-I or emerging thermokarst (n=2), seepage-II or slow discharging spring (n=4), spring (n=17) and groundwater (n=13). The main branch of Heihe river to which the HLGW tributaries converge were also sampled (n=3). The meltwater sample was collected in triplicate from headwaters generating from glacier-snow melting in bare gravel zone at an elevation of 4100 m. Stream water samples were collected from the east and the west tributaries originating at high mountains above 4765 m, from the mid-stretch after the east and the west tributaries converge, and from the lower stretch after the red mud gully joins in. Red mud gully is an erosional tributary; formed by water cutting deeply into the degraded seasonally frozen soil zone in the alpine meadow at an altitude between 3300 m to 3000 m a.s.l, and thus classified separately as a type of water. Thawing of permafrost results in many small thermokarst ponds (diameter < 1 m mostly), observed in the alpine meadow at an altitude ranging from 3351 m to 3548 m close to the east tributary. Groundwater samples were collected from the WW1, WW3, WW4 and MW wells (Fig. 1d, see Supporting Information Dataset S1 for depth). Sample collection method is described in Text S1 of Supporting Information.

2.2 Measurements of field and chemical parameters, stable isotopes and DOM

Temperature (T), electrical conductivity (EC), pH and alkalinity were measured in the field. Stable isotopes (δD and δ^{18}O) were measured on a water isotope spectrometer analyzer (Model PICARRO L2130-I) at Pri-ecoco, Beijing, China. Major anions and cations of samples in 2012 and 2013, were measured by ion chromatography (IC-1000, Dionex) and Inductively Coupled Plasma Atomic Emission Spectroscopy (ICPAES, Teledyne Leeman, Prodigy), respectively. Major ions of sample in 2018 were measured on IC (Aquion, Dionex) with CS18 analytical column for anions, and CS16 column for cations, respectively. DOC concentrations of all water samples and soil extraction solutions (see Text S2 and Fig. S1 of Supporting

Information on soil incubation) were measured on a Shimadzu TOC Analyzer. Detailed procedures are in Text S1 of Supporting Information.

UV abundance of chromophore DOM (CDOM) was measured by a UV-Visible Spectrophotometer (Agilent 8453) scanning from 200 to 800 nm (1 nm increments) for samples collected in 2012 and 2013. Prior to analyzing samples, a quartz cuvette filled with Milli-Q water was used to establish a daily baseline. Excitation emission matrices (EEMs) were employed by scanning over an excitation (ex) range of 240 to 450 nm at 10 nm increments, and an emission (em) range of 350 to 550 nm at 2nm increments on a JY-Horiba Fluoromax-3 spectrofluorometer (Queens College, CUNY) with instrument-specific corrections, Raman normalization, inner filter correction, and cuvette blank subtraction applied. Optical properties of samples collected in 2018 were analyzed using a Horiba Aqualog spectrofluorometer (Southern University of Science and Technology) following the same procedure. EEMs were generated over excitation wavelengths between 246.58 to 827.57 nm in about 1.2–nm interval and emission wavelengths between 220 to 800 nm in 1-nm interval.

To correct for minor effect of light scattering by particles and microbubbles, wavelength-independent correction is conducted by subtracting the mean absorbance at range of 600 to 800nm from all spectral absorbance values [*Green and Blough*, 1994]. Specific UV absorbance ($SUVA_{254}$) which can fingerprint aromatic substance in DOM, was calculated following previously reported methods [*Weishaar et al.*, 2003]. Fluorescence index (FI) is calculated as the ratio of intensities emitted at 470 nm and 520 nm at an excitation wavelength of 370nm, which has been found to be a stable and robust indicator of terrestrial (~1.2) and microbial (~1.8) DOM sources [*Cory and McKnight*, 2005; *McKnight et al.*, 2001]. Freshness index (BIX) is calculated as the ratio of emission intensity at 380 nm to the maximum intensity between 420 nm and 435 nm at an excitation wavelength of 310 nm, and refers to recently produced organic matter [*Parlanti et al.*, 2000].

2.3 Parallel Factor Analysis (PARAFAC) of DOM Fluorescence Spectra

Fluorescence spectra, obtained as EEMs, are used to quantify the contribution of fluorescent DOM components, including protein-like fluorophores, through PARAFAC modeling [*Coble*, 1996; *Murphy et al.*, 2013]. The EEMs of CDOM in water samples were first corrected for instrumental differences with user-generated excitation, emission and lamp intensity correction factors. After blank subtraction, they were normalized to water Raman units (RU).

Parallel factor analysis was conducted following the procedures described in a previous algorithm to quantify the protein-like and humic-like substances of DOM [*Murphy et al.*, 2013; *Stedmon and Bro*, 2008]. Prior to outlier tests, the intensity of EEMs of samples in 2018 was linearly interpolated to match the emission ranging 250 to 450 nm at an interval of 10 nm and excitation ranging 300 to 550 nm at an interval of 2 nm. To avoid highly fluorescent samples exerting significant leverages on the PARAFAC model, normalization of each EEM to its integrated fluorescence was applied before model fitting [*Murphy et al.*, 2013]. Normalized fluorescence of each EEM was reversed to its raw fluorescence after model fitting.

A series of three to six component models were fitted to the dataset, with non-negativity constraint of 10^{-8} applied. The split-half validation was achieved through splitting the data in half

and modeling each half separately, fitting 20 models with random starts, and by inspection towards lowest residuals [*Murphy et al.*, 2013]. The PARAFAC analysis resolved a four-components model comprising the EEMs dataset, explaining 97.8% of the total variance. Spectra loadings of both excitation and emission mode for each component were matched to the OpenFluor database, and the description of each component was interpreted from matched compounds identified from previous studies with similarity >95% [*Murphy et al.*, 2014]. The identified four fluorescence components (C1 to C4) are ubiquitous and common in marine environments [*Catala et al.*, 2015; *Wunsch et al.*, 2018], as well as cryosphere such as Arctic surface waters [*Gonçalvesaraujo et al.*, 2016] and ice cores in Arctic Canada [*Brogi et al.*, 2018], and ice in the Antarctic seas [*Stedmon et al.*, 2011]. The C1 and C3 components have a broader emission spectrum and two extraction spectra peaks, traditionally referred to as humic-like components (Fig. S2). The C2 (ex: 270 nm; em: 304 nm) and C4 (ex: 290 nm; em: 338) components have narrower spectra with excitation and emission maxima below 350 nm (Fig. S2), and are similar to the spectra of tyrosine and tryptophan, respectively [*Murphy et al.*, 2008]. The characterization of C2 and C4 represents amino-acids, free or bound in proteins compounds. The proportion of protein-like fluorophores is calculated as the sum of C2 and C4 intensities divided by the bulk intensity of the sample.

2.4 End Member Analysis Based on Conservative Tracers

A three end-member mixing analysis constrained by "conservative" tracers δ^{18}O and EC was used to calculate the proportions of glacier-snow (f_G), precipitation (f_P) and frozen soil melt water (f_s) contributing to stream and subsurface waters in HLGW. The analysis is based on the following assumptions: (1) the three water sources are the dominant sources over the ablation season and that any other sources are negligible; (2) shallow, organic layer of frozen soil is involved in lateral flow thus provides a signature representing this endmember.

$$f_G \times C_G^{18O} + f_P \times C_P^{18O} + f_S \times C_S^{18O} = C_i^{18O} \quad (1)$$

$$f_G \times C_G^{EC} + f_P \times C_P^{EC} + f_S \times C_S^{EC} = C_i^{EC} \quad (2)$$

$$f_G + f_P + f_S = 1 \quad (3)$$

where f represents the estimated fraction of a given endmember contributing to the specific sample i; the subscripts G, P and S represent the glacier-snow meltwater, precipitation and soil endmember, respectively; C^{18O} and C^{EC} represent the δ^{18}O and EC of the sample specified in the subscript, respectively.

The δ^{18}O and EC values to constrain the glacier-snow endmember composition rely on three meltwater samples analyzed in this study, two newly deposit snow samples in May and November of 2012 and one meltwater sample in July 2012 in the front of glacier in HLGW [Li et al., 2015] (Table S1). Mean EC and δ^{18}O averaged from 65 rainwater samples at different elevations (2960 to 4160 m a.sl.) of HLGW are used to represent the precipitation endmember [Chang et al., 2018] (Table S1). The compositions of the frozen soil melt water endmember are averaged from mean values of 87 samples collected underneath the soil profile in different elevation of HLGW in Li et al [Li et al., 2014], and includes also four soil samples collected and analyzed similarly in this study (Table S1).

To estimate the uncertainty associated with the tracer-based end-member analysis, a classical Gaussian error propagation equation was employed [*Genereux*, 1998; *Uhlenbrook and Hoeg*, 2003]. The calculation followed procedure described elsewhere [*Chang et al.*, 2018]. The fractions and associated uncertainties are reported in Table S2.

$$W_f = \left[\left(\frac{\partial f}{\partial C_G^{18O}} W_G^{18o}\right)^2 + \left(\frac{\partial f}{\partial C_P^{18O}} W_P^{18o}\right)^2 + \left(\frac{\partial f}{\partial C_s^{18O}} W_s^{18o}\right)^2 + \left(\frac{\partial f}{\partial C_i^{18O}} W_i^{18o}\right)^2 + \left(\frac{\partial f}{\partial C_G^{EC}} W_G^{EC}\right)^2 + \left(\frac{\partial f}{\partial C_P^{EC}} W_P^{EC}\right)^2 + \left(\frac{\partial f}{\partial C_s^{EC}} W_s^{EC}\right)^2 + \left(\frac{\partial f}{\partial C_i^{EC}} W_i^{EC}\right)^2\right]^{1/2} \quad (4)$$

where W represents the uncertainty in the variable specified in the subscript, i.e W_f represents the uncertainty of the contribution fraction for a given end member in a sample, W_G^{18o} represents the uncertainty of δ^{18}O in glacier-snow endmember.

2.5 Estimation of DOC Loss: ΔDOC

Because DOC is non-conservative, we first estimate an initial DOC (DOC_0) through summation of DOC contributed from each endmember (equation 5).

$$DOC_0 = f_G \times DOC_G + f_P \times DOC_P + f_S \times DOC_S \quad (5)$$

The DOC concentration (0.5 ± 0.02 mg L^{-1}) in meltwater at the highest elevation is taken to represent the glacier-snow endmember (Table S1). The DOC concentration (15 ± 2.5 mg L^{-1}) of samples collected from four soil profiles at a depth of 5 cm below ground (see Text S2 for soil sampling) is taken to represent the soil endmember (Table S1). Though DOC of rainfall was not measured in HLGW, the volume-weighted mean DOC is 0.9 mg L^{-1} in three remote meteorological stations and 1.1± 0.5 mg L^{-1} in Lhasa city of central QTP [*Li et al.*, 2018; *Wang et al.*, 2017]. The DOC of 1.0 mg L^{-1} is taken to represent the precipitation endmember (Table S1).

The difference between initial DOC and measured DOC of a sample suggests the loss of carbon along the flowpath of water to the sampling point. The DOC loss (ΔDOC) is calculated by subtracting measured DOC concentration ([*DOC*]) of a given water sample from its initial DOC (DOC_0) calculated above, where larger ΔDOC corresponds to more loss of DOC during transport.

$$\Delta DOC = DOC_0 - [DOC] \quad (6)$$

2.6 Estimation of Groundwater Mean Transit Time

The first order kinetics has been widely used to describe biodegradation of DOC incubation experiments [*Catala et al.*, 2015], allowing for calculation of the degradation rate constant (λ) as in equations (7), where the DOC_0 usually represents the starting point of the experiment.

$$DOC = DOC_0 \times e^{-\lambda \times t} \quad (7)$$

Because photodegradation is unlikely in subsurface environment, the biodegradation rate constant is assumed to regulate DOC degradation in groundwater. Re-arranging equation (7) to simulate the ΔDOC change in groundwater observed at the outlet of HLGW in July and September result in equation (8), with the calculated time, t, regarded as representing groundwater mean transit time (MTT).

$$1 - {\Delta DOC}/{DOC_0} = e^{-\lambda_{gw} \times t} \quad (8)$$

$$MTT \approx t = -\frac{\ln(1-{\Delta DOC}/{DOC_0})}{\lambda_{gw}} \quad (9)$$

where λ_{gw} represents DOC degradation constant in groundwater which has been corrected to observed groundwater temperature of 5 ^{o}C based on the Arrhenius equation [*Catalan et al.*, 2016] from the incubation experiment temperature of 20 ^{o}C.

3 Results

3.1 Frozen Soil Meltwater Contributes to All Water Types

Stable isotope characteristics of eight types of water indicate the influence of not only glacier-snow meltwater (G) and precipitation (P) but also frozen soil melt water (S) endmember (Figs. 2a and 2b). Stream and subsurface water (groundwater, spring and seepage-II) samples fall within the triangle defined by the G, P and S endmembers (Figs. 2a and 2b). The regression line of meltwater, stream, seepage-II, spring and groundwater ($8.07 \times \delta^{18}O + 20.79$, r^2=0.92, n=71, blue line in Fig. 2a) is similar to the local meteoric water line (LMWL: $8.5 \times \delta^{18}O + 22.6$, gray line in Fig. 2a) of HLGW [*Ma et al.*, 2017]. In contrast, thermokarst pond waters, two seepage-I samples and red mud gully waters exhibit more positive isotopic compositions and fall below the local meteoric water line (LMWL) on a different trend line ($5.16 \times \delta^{18}O - 1.13$, r^2=0.83, n=20, black line in Fig. 2a), indicating fractionation due to evaporation. The red mud gully waters are most similar to the frozen soil melt water endmember in compositions (Fig. 2b); and this is interpreted to indicate that red mud gully waters are derived from the frozen soil melt water. The two seepage-I samples (emerging thermokarst) represent mixing between roughly 25%±1% of the soil endmember, and 75%±1% of the precipitation endmember, respectively (Fig. 2b). The thermokarst pond waters are also likely a mixture of the S and P endmembers, although the isotopic values have become more positive due to evaporation. In summary, red mud gully, emerging thermokarst (seepage-I) and thermokarst ponds all have significant frozen soil meltwater contribution.

Using EC and $\delta^{18}O$ to un-mix among the three endmembers for stream and subsurface water (groundwater, spring, and seepage-II) samples falling within the triangle, precipitation contributes on average about 62%±7%, 64%±4%, 61%±4% and 63% of the water in stream, groundwater, spring, and seepage-II, respectively (Fig. 2b). Glacier-snow meltwater ranked second for stream (28%±6%), groundwater (18%±4%) spring (24%±4%) and seepage-II (26%). The smallest component is frozen soil meltwater, contributing the least (10%±4%) to the stream, but increases to 11%, 15%±5%, and 17%±2% in seepage-II, spring, and groundwater, respectively.

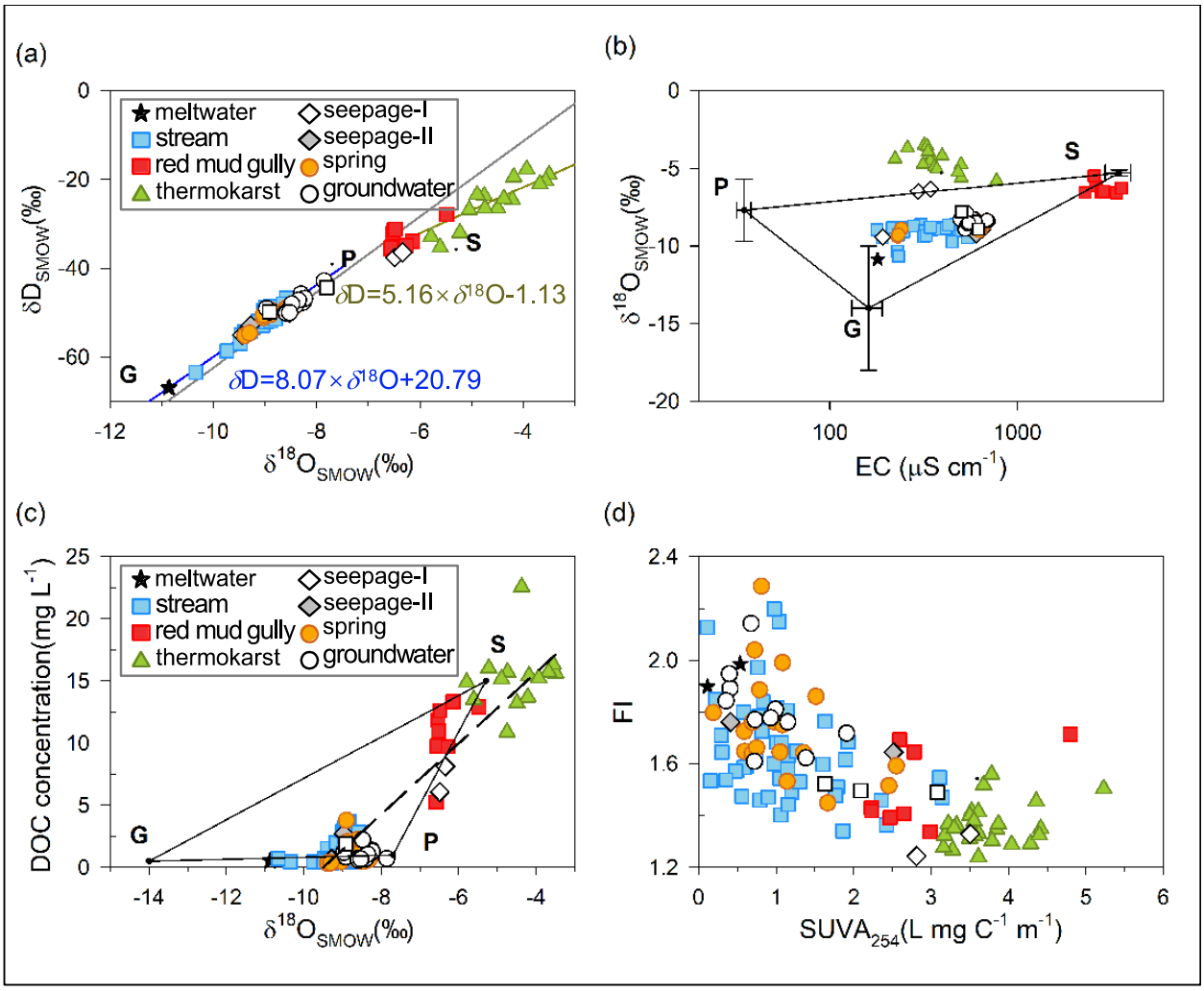

Figure 2. (a) Stable isotope compositions ($\delta^{18}O$ and δD) of eight types of water in HLGW. Three endmembers: glacier-snow meltwater (G), precipitation (P) and frozen soil meltwater (S) are marked according to their compositions. Local meteoric water line (LMWL: 8.5 × $\delta^{18}O$ + 22.6) is shown as a gray line [*Ma et al.*, 2017]. (b) The $\delta^{18}O$ vs electrical conductivity (EC, log scale) of eight types of water samples from HLGW. The triangle outlines the three end members with the error bar representing standard deviation for the two tracers. Uncertainties in $\delta^{18}O$ and EC of the three endmembers are reported in Table S1. (c) The $\delta^{18}O$ vs DOC concentrations for all eight types of water within HLGW are shown with positive relation ($p<0.01$; $n = 103$). The triangle outlines the three end members according to their $\delta^{18}O$ and DOC concentrations. (d) The $SUVA_{254}$ vs FI for all eight types of water ($r = –0.59$, $p = 0.01$).

3.2 Thawing of Frozen Soil Supplies Most DOM to Surface and Subsurface Waters

Several lines of evidence suggest that DOM in surface water has been influenced by DOM from thawing of seasonal frost and/or permafrost soil. Three types of water show high DOC levels (Table 1): thermokarst ponds (14.3 ± 3.3 mg L^{-1}, n=26), red mud gully (10.8 ± 2.5 mg L^{-1}, n=10) and seepage-I (7.1 ± 1.4 mg L^{-1}, n=2). The elevated DOC levels of these three types of water are consistent with the large contribution of frozen soil melt water endmember (Fig. 2b). These waters also show the most positive $\delta^{18}O$, with a correlation with DOC concentrations (Fig. 2c). Because DOC concentrations in glacier-snow (0.5 mg L^{-1}) and precipitation (1 mg L^{-1}) endmembers are low, this means that DOC in the stream (1.3±1.1 mg L^{-1}, n=41), spring (1.1±1.1 mg L^{-1}, n=17), groundwater (1.1±0.4 mg L^{-1}, n=13) and seepage-II (1.5±0.8 mg L^{-1}, n=4) must include a source from thawing of frozen soil, consistent with the water source analysis results above. When the DOC concentrations of all samples are divided into tertile (Fig. 1a), stream waters (n=29) with low DOC level (0.7±0.3 mg L^{-1}) display the most negative $\delta^{18}O$ values of –9.20±0.48 ‰ while stream waters (n=12) with medium DOC level (2.9±0.7 mg L^{-1}) show in-between $\delta^{18}O$ of –8.82±0.14 ‰, indicating input of frozen soil-derived DOC to streams.

Table 1. Electrical conductivity (EC), isotopic compositions, DOC concentration and optical properties in eight types of water in HLGW.

Type	n	Elevation (m)	EC (μs cm^{-1})	$\delta^{18}O$ (‰)	δD (‰)	DOC (mg L^{-1})	Protein proportion (%)	$SUVA_{254}$ (L mgC^{-1} m^{-1})	FI	BIX
Meltwater	1	4100	179±1	-10.6±0.5	-64.8±3.8	0.5±0.0	51±3	0.33±0.17	1.94±0.04	0.83±0.02
Stream	41	3620-2920	355±141	-9.1±0.4	-52.1±4.6	1.3±1.1	56±33	1.09±0.63	1.62±0.16	0.73±0.14
Seepage-II	4	3410-3060	501±181	-9.1±0.4	-52.2±2.0	1.5±0.8	43±39	1.16±0.80	1.60±0.16	0.61±0.12
Spring	17	3570-2950	450±196	-8.7±0.3	-50.1±2.2	1.1±1.0	59±31	1.14±0.60	1.75±0.21	0.74±0.21
Groundwater	13	3300-2970	573±61	-8.5±0.3	-48.0±2.1	1.0±0.4	62±24	0.88±0.45	1.82±0.14	1.12±0.38
Thermokarst ponds	26	3620-3350	334±123	-4.5±0.7	-24.8±5.3	14.3±3.3	24±11	3.75±0.48	1.37±0.09	0.59±0.05
Red mud gully	10	3200-3050	2881±399	-6.3±0.4	-32.8±2.5	10.8±2.5	30±14	2.84±0.78	1.50±0.14	0.71±0.09
Seepage-I	2	3610	322±25	-6.4±0.1	-37.1±0.6	7.1±1.0	45±22	3.16±0.35	1.29±0.04	0.58±0.03

Note. Elevation is reported as range. Data are reported as averages ± standard deviation for each water type. Meltwater was collected in triplicate.

Further support for the importance of thawing supplied DOM in the watershed is based on characterization of the quality of DOM by UV-vis and fluorescence spectroscopy because of its ability to absorb light and fluoresce. The optical properties including $SUVA_{254}$, FI and BIX all

point to various degrees of influence by DOM from thawing of seasonal frost and/or permafrost soil. Thermokarst, red mud gully and seepage-I (emerging thermokarst) waters characterized by elevated DOC concentration display the highest $SUVA_{254}$ and the lowest FI values (Fig. 2d and Table 1). This indicates overwhelming influence by terrestrial plant-soil sourced DOM with high aromaticity from organic matter produced some time ago. The glacier-snow meltwater is the least likely to be influenced by any DOM from frozen soil melt, and thus shows the lowest $SUVA_{254}$ (0.33±0.17 L mgC^{-1} m^{-1}) and the highest FI (1.94±0.04). Stream, spring and groundwater display $SUVA_{254}$ and FI values between the aforementioned two DOM optical "endmembers" (Fig. 2d). Subsurface waters (spring and groundwater) show higher BIX and FI values than stream water, indicating recent microbially processed DOM [*Parlanti et al.*, 2000], consistent with the interaction with microbes in subsurface environment. The BIX values of meltwater, groundwater, and most spring water lie above the median BIX value of 0.69 of the all eight types of water, while those of most stream, red mud gully, seepage-I and thermokarst pond waters are below (Fig. S4).

3.3 Differences in DOM quality in Surface and Subsurface Waters

The proportion of protein-like fluorophores in DOM, which has been widely considered as a proxy for labile DOM (eg. [*Balcarczyk et al.*, 2009; *Fellman et al.*, 2010; *Fellman et al.*, 2008]), is overall high but spatially variable in surface and subsurface waters of HLGW (Fig. 1b) based on a four-component PARAFAC model (Fig. S2). The DOM of meltwater collected at the origin of east tributary displays low $SUVA_{254}$ of 0.33±0.17 L mg C^{-1} m^{-1} and 51±3% of protein-like fluorophores, respectively (Figs. 1b and Table 1). These values are comparable to that of glacier-snow meltwater (n=2) in southwest QTP, with $SUVA_{254}$ of 0.60 L mg C^{-1} m^{-1} and >50% of amino-acids [*Spencer et al.*, 2014; *Xu et al.*, 2013]. Although the meltwater can be a source of "labile" DOC, its DOC concentration is also the lowest among the eight types of water; thus, there must be additional "labile" DOC from other sources. Three types of water, including thermokarst, red mud gully and seepage-I, contain high DOC with substantial (though variable) proportions of protein-like fluorophores of 24±11% (n=12), 30±14% (n=8), and 45±22% (n=2), respectively (Table 1). Thus, the quantity of "labile" C is substantial and is a source for other water types. Representative EEMs of different water types are shown in Fig. S3 of Supporting Information.

The first piece of evidence for "labile" DOC sourced from thawing is the differences in quantity and quality of DOC in surface water between the east and the west tributaries in the upper stretch of the HLGW. Concentrations of DOC and proportions of protein-like components are on average higher in the east tributary (1.7±1.3 mg L^{-1}, 69±30%, n=21) that drains two areas of permafrost and seasonal frost areas than those in the west tributary (0.8±0.3 mg L^{-1}, 46±31%, n=13) that drains only one smaller area of permafrost (Fig. 1d and Table 2). Subsurface waters of the upper stretch display lower DOC concentration than surface water (Fig. 1a), with comparable protein-like proportions (Fig. 1b and Table 2).

Table 2. DOC concentrations, optical properties of DOM, proportions of glacier-snow (f_G), precipitation (f_P) and soil water (f_s) contributing to stream and subsurface waters and associated DOC loss for the upper, mid and lower stretch of HLGW.

Category	Type	n	DOC (mg/L)	Protein proportion (%)	$SUVA_{254}$ (L mg^{-1} C^{-1} m^{-1})	FI	f_G	f_P	f_S	DOC_0 (mg/L)	ΔDOC (mg/L)
Upper stretch: east tributary (3620-3190 m)	surface	21	1.7±1.3	69±30%	1.18±0.60	1.60±0.14	29±9%	62±9%	10±4%	2.2±0.6	1.2±0.8
	subsurface	9	1.2±0.9	57±20%	1.38±0.73	1.71±0.11	19±2%	64±4%	17±2%	3.3±0.3	2.3±0.5
Upper stretch: west tributary (3500-3180 m)	surface	13	0.8±0.3	46±31%	1.12±0.75	1.62±0.20	27±3%	65±3%	8±2%	2.0±0.3	1.2±0.5
	subsurface	3	0.4±0.0	47±14%	1.00±0.37	1.85±0.15	27±4%	59±5%	13±6%	2.7±0.8	2.3±0.8
Mid-stretch (3140-3040 m)	surface	8	1.1±0.7	43±30%	0.77±0.24	1.66±0.10	27±3%	58±3%	16±2%	3.0±0.3	1.9±0.5
	subsurface	4	1.2±0.5	85±14%	1.00±0.16	1.69±0.18	22±3%	64±3%	14±5%	2.9±0.8	1.7±0.9
Lower stretch (3000-2940 m)	surface	3	1.3±0.8	44±31%	0.76±0.21	1.67±0.12	26±2%	60±5%	14±3%	2.8±0.4	2.4±0.1
	subsurface	13	1.2±1.0	57±31%	0.81±0.40	1.84±0.21	22±4%	62±4%	15±3%	3.1±0.5	2.2±0.7

Note. Surface represents stream and subsurface includes spring and groundwater. Data are reported as averages ± standard deviation for each category.

In the short mid-stretch after the east and west tributaries converge, the stream DOC (1.1±0.7 mg L^{-1}, n=8) reflect mixing of upstream waters from the east and west tributaries (Fig. 1a). However, simultaneous reductions in protein-like proportion to 43±30% and in $SUVA_{254}$ values to 0.77±0.24 L gC^{-1} m^{-1} (Table 2) indicate in-stream DOC processing. The $SUVA_{254}$ values of the four subsurface water samples in the mid-stretch are higher than those of the stream waters (Table 2). The proportion of protein-like fluorophores (85±14 %, n=4) nearly double that of stream water (Fig. 1b).

In the lowest stretch, the stream DOC increases to 1.3±0.8 mg L^{-1} (n=3) after the convergence of red mud gully characterized by high DOC level. The mean protein-like proportions of 44±31% and $SUVA_{254}$ of 0.76±0.21 L mgC^{-1} m^{-1} are similar to those of the mid-stretch (Fig. 1b and Table 2). The DOC concentrations (1.2±1.0 mg L^{-1}) and variable protein-like proportions (57±31%, range: 18%–99%) in subsurface waters (n=13) are similar to those from the highest elevation area, but lower than those the mid-stretch, suggesting a groundwater flow path may connect the highest elevation area with the lowest stretch whereas the mid-stretch may have been influenced more by a cluster of thermokarst ponds nearby (Figs. 1a and 1b).

In each stretch of HLGW stream network, the mean value of FI in subsurface waters is higher than that in the surface waters (Table 2), indicating more microbially processed DOM in subsurface environment. When protein-like proportion is divided into tertile of all samples, all of 12 groundwater samples, and 10 out of 13 spring samples belong to medium and high levels (Fig. 1b). The spring waters also have the highest bulk fluorescence intensity averaging 3.85 ± 6.58 RU (Dataset S2). Taken together, the differences in DOM quality in surface and subsurface waters, along with the spatially variable distribution of protein-like fluorophores, suggest that subsurface environment actively participate in DOM processing in headwaters of the QTP.

4 Discussion

4.1 Labile DOC Losses in HLGW: ΔDOC

Beyond optical properties of DOM indicative of prevalence of bioavailable DOM in HLGW, ΔDOC that represents DOC loss is estimated to evaluate to what extent DOM in HLGW is "labile". Because the frozen soil endmember contains much more DOC than the glacier-snow and precipitation endmembers do, the uncertainty in ΔDOC estimation is small and is mostly driven by the very small uncertainty of the soil endmember (Table S2). Although glacier-snow and precipitation endmembers exhibit substantial uncertainties in their compositions (Table S2) due to altitudinal and temporal effects on isotopic compositions [*Chang et al.*, 2018; *Li et al.*, 2015], their effect on uncertainties of ΔDOC estimation is insignificant due to their low DOC content.

In stream water, the proportion of protein-like fluorophores decreases from almost 100% to ~ 20% with increasing ΔDOC (Fig. 3a). There is, however, no clear trend in $SUVA_{254}$ values with increasing ΔDOC (Fig. 3b). This is consistent with prior studies showing that both biodegradation and photodegradation are important for mineralization of permafrost derived DOM in surface waters. In high-altitude or high-latitude aquatic environments, photodegradation dominates in-stream DOC processing due to availability of sunlight. For example, photochemical removal of DOM is responsible for 70–95% of the total DOM degradation across first-to-third-order rivers in the Arctic region, with the rate of photodegradation 5 times higher than that of microbial respiration [*Cory et al.*, 2014]. Selectively leached aromatic carbon from shallower organic layer is preferentially photodegraded whereas the protein-like fraction released from deeper layers is preferentially biodegraded [*Ward and Cory*, 2015; *Wang et al.*, 2018a]. In the upper stretches of the stream network in HLGW, the proportions of protein-like fluorophores decrease also with increasing ΔDOC, although only the upper west tributary exhibits decreasing $SUVA_{254}$ values with increasing ΔDOC over ~ 1 km distance (Fig. S5). Like the DOC loss in these first-order mountain streams of HLGW, a recent study in Gangcha County of the QTP also shows that half of the DOC is "lost", accompanied by halving of $SUVA_{254}$ value in a 2.5-km stream flowing through a thermo-erosion gully (elevation: 3850 to 3200 m a.s.l) [*Wang et al.*, 2018b].

In subsurface waters, simultaneous decreases in the proportions of protein-like fluorophores and $SUVA_{254}$ values are observed with increasing ΔDOC. For groundwater, the linear correlation coefficients are 0.58 for protein-like proportion (Fig. 3a) and 0.41 for $SUVA_{254}$ (Fig 3b) respectively. The consumption of aromatic carbon and protein-like fluorescent DOM is also supported by incubation experiments of seasonal frost and permafrost soils from HLGW conducted in dark (Table S3). Together, the results support the notion that aromatic DOM with high protein-like fluorophores, most likely sourced from thawing of frozen soil, is "labile" and is mineralized in subsurface environment of the HLGW. Subsurface DOM is much less likely to undergo photo-oxidation or mineralization by sunlight, the DOC loss is therefore considered to mostly reflect biodegradation. While we cannot entirely rule out the possibility of photodegradation due to frequent surface and subsurface water exchanges in HLGW, the MTT (mean transit time) of subsurface water should be longer than that of stream water, allowing for microbial processing time of DOM in subsurface environment. The longer the processing time is, the higher the DOC loss by microbial activities will be along the subsurface flow path. We take advantage of this linkage to calculate MTT of groundwater using its ΔDOC obtained at the outlet

of HLGW as discussed in 4.2 next. The MTT reflects the flow pathways and water dynamic of the whole system [*McGuire et al.*, 2005].

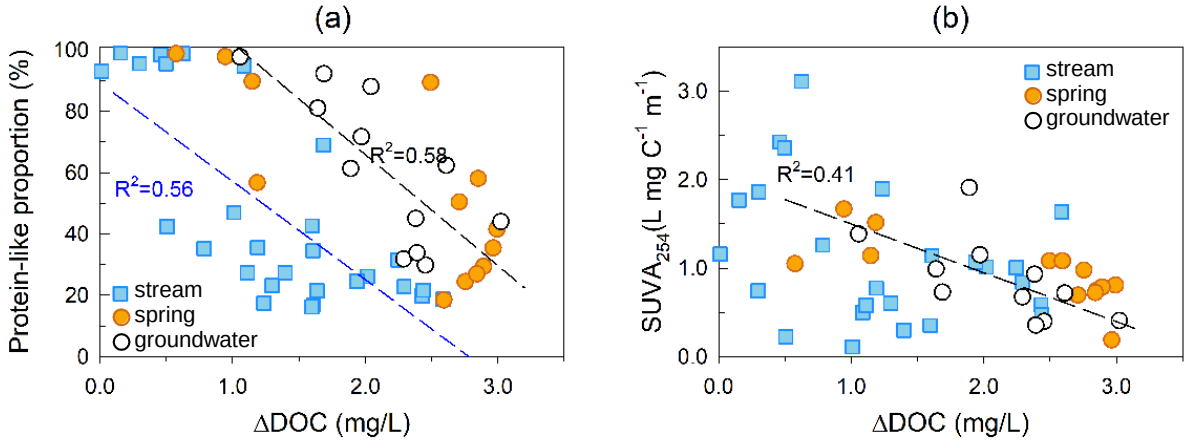

Figure 3. (a) The proportion of protein-like component vs DOC loss (ΔDOC) in surface (blue) and subsurface (white and orange) water. (b) $SUVA_{254}$ vs DOC loss (ΔDOC) in surface (blue) and subsurface (white and orange) water. The blue and black dash lines represent the regression lines for stream and groundwater, respectively, with correlation coefficients marked next to the lines.

4.2 Groundwater Mean Transit Time (MTT) in Response to Freeze-Thaw Cycles

Prior studies in the Artic region have found low percentages of protein-like fluorophores: 0.3–22% in eight streams extending 250 km at Yenisei basin [*Kawahigashi et al.*, 2004; *Mann et al.*, 2012]; 1–12% over 500 km at Yukon basin and its small tributaries [*Cory et al.*, 2007; *O'Donnell et al.*, 2010; *Wickland et al.*, 2012]. In the Arctic permafrost region, groundwater discharge is driven by soil freeze – thaw processes with long water retention time [*Ameli et al.*, 2017; *Ireson et al.*, 2013; *Walvoord and Striegl*, 2007] and horizontal flow path [*Aiken et al.*, 2014; *O'Donnell et al.*, 2012]. HLGW is small (25 km^2) and alpine (11° topographical gradient) so the groundwater MTT is expected to be rapid though not previously quantified. Only a handful of studies have attempted to quantify mean transit time in hillslopes. MTT of days to weeks (10 – 25 days) has been obtained for storm events, based on hydrometric and isotopic tracer approach in an alpine watershed of Oregon [*McGuire and McDonnell*, 2010]. Very short transit time of 2 to 12 days is observed for a mountain spring in Hong Kong constrained by radium (Ra) and radon (Rn) isotopes along a steep slope [*Luo and Jiao*, 2019].

In the following, we first discuss qualitative evidence for MTT of groundwater in HLGW responding to the seasonal freeze-thaw cycles followed by an attempt to quantify the MTT in low and high discharge periods.

First, DOC concentrations of groundwater and spring collected at the same locations close to the outlet of HLGW reach a maximum in July during peak discharge, higher than those in September when discharge is much less (Fig. 4). The ΔDOC of these subsurface waters are 1.0±0.1 mg L^{-1} in July and 2.5±0.4 mg L^{-1} in September, respectively, suggesting lower loss in July than in September. This contrast is neither attributable to a difference in DOC_0 (July:

3.2±0.04 mg L^{-1}; September: 3.2±0.2 mg L^{-1}) nor to water temperature (5 °C). It is unlikely due to adsorption alone because DOM adsorption is rapid, and usually reaches equilibrium within a few minutes to hours [*Gu et al.*, 1994; *Kalbitz and Wennrich*, 1998].

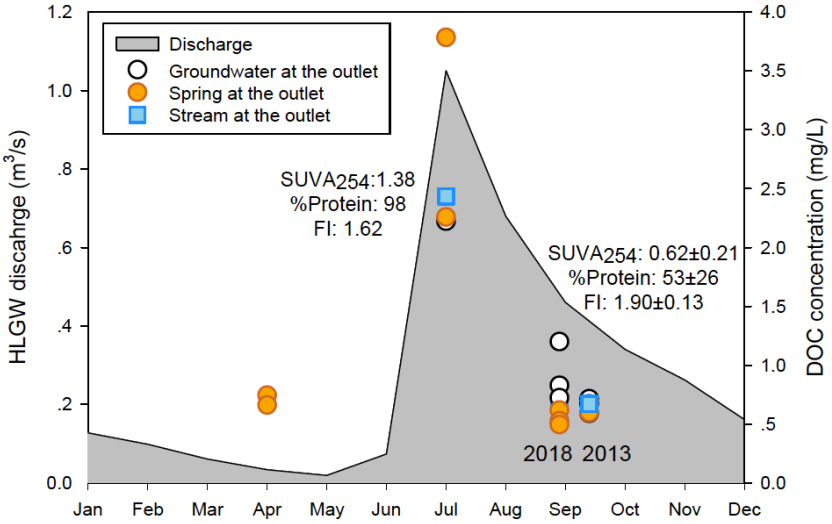

Figure 4. Monthly average stream discharge (left y-axis) in 2013 displayed in gray shade recorded at the gauging station (2960 m a.s.l) at the outlet of HLGW. Concentrations of DOC (right y-axis) in surface water (blue square) and springs (orange circles) and groundwater (white circles) from a monitoring well (MW – 30 m depth in Fig. 1d), all close to the gauging station, are higher in July than in September. Numbers are values of $SUVA_{254}$ (L mg C^{-1} m^{-1}), proportion of protein-like compound (%) and FI for groundwater from the MW.

Second, the protein-like proportion and $SUVA_{254}$ of all subsurface waters at the outlet are higher in July (98±0.5%, 1.25±0.41 L mg C^{-1} m^{-1}, n=3) and lower in September (45±23%, 0.66±0.26 L mg C^{-1} m^{-1}, n=10). The inferred shorter MTT in July allows for more "labile" DOM to be detected in the subsurface environment. This change is especially clear when groundwaters repeatedly sampled from a single monitoring well screened at 30 m depth below ground (MW, see Fig.1d) in July 2013, September 2013 and 2018 are considered (Fig. 4). Moreover, the DOC contrast in surface water is also consistent with this difference in transit time (Fig. 4). The higher discharge and thus more extensive surface water and groundwater interaction in July compared to September accelerates the already rapid downward flow of groundwater in HLGW, also supported by field observation of the spring discharge at the outlet of HLGW.

Third, an attempt is made to estimate groundwater MTT based on the DOC dynamics described above, assuming subsurface biodegradation of labile DOC with first order kinetics. Though incubation studies of Arctic water DOM have found variable λ of 5×10^{-3} to 0.15 d^{-1} [*Balcarczyk et al.*, 2009; *Fellman et al.*, 2008; *Fellman et al.*, 2009; *Spencer et al.*, 2014], 0.15 d^{-1} is most likely to be representative of highly labile and freshly released DOC in headwaters at 20°C. Incubations of HLGW soils have found a degradation constant (λ_{SOC}) of 0.32 d^{-1} at room temperature (see Text S3 and Fig. S6 in supporting information for details). The biodegradation constant (λ) of 0.15 d^{-1} established from the incubation of DOM in first-order streams of the

Kolyma River [*Spencer et al.*, 2015] becomes 0.05 d^{-1} after correcting to HLGW groundwater temperature of 5°C following the Arrhenius equation [*Catalan et al.*, 2016]. Using 0.05 d^{-1}, the MTT is estimated to be approximately 7 days and 25 days in July and September, respectively, corresponding to the changes in ΔDOC (ΔDOC/DOC_0) observed for groundwater of monitoring well at HLGW outlet of 32% in July and 74% in September (Fig. 5). Because most labile DOC entered the aquatic environment in the upper stretch of HLGW (Fig. 1), this estimation of reaction time based on DOC degradation is thus indicative of MTT for groundwater in HLGW.

Based on temperature corrected soil carbon degradation constant (λ_{SOC}) of 0.11 d^{-1} at 5°C from our HLGW soil incubation experiment established 0.32 d^{-1} at 20°C (Text S3), the MTT is estimated to be 3.5 d and 12.5 d for July and September, respectively (Fig. 5). Based on the slowest λ (5×10^{-3} d^{-1}) reported for incubation of DOM in the stream waters from Alaska at 4°C with in situ nutrients [*Balcarczyk et al.*, 2009], the MTT can be as long as 200 d for July and 700 d for September, respectively (Fig. 5). Given the degrees of spatial and temporal variability in DOM quantity and quality, biodegradation and sorption kinetics of DOM warrant further investigation to improve the estimation of groundwater transit time that can also benefit from an independent assessment using Ra-Rn isotopes [*Luo and Jiao*, 2019]. Further, changes in DOC and $SUVA_{254}$ from our soil incubation experiments suggest release of aromatic carbon (Table S3). This raises the yet to be assessed possibility that preferential sorption of highly aromatic carbon or humic-like compounds onto soil or sediment may contribute to DOC loss along the groundwater flow path [*Jin and Zimmerman*, 2010]. Finally, long-term observations of DOM quantity and quality are desirable to reveal DOM dynamics that will allow separation of effects of gradual, seasonal freeze-thaw cycles and abrupt, accelerated thawing of permafrost. These limitations are unlikely to challenge the assumption that subsurface DOM is primarily driven by biodegradation, and the rate constants are similar in July and September. If so, the results are interpreted to suggest that MTT in hillslopes vary in response to discharge corresponding to season freeze-thaw cycles.

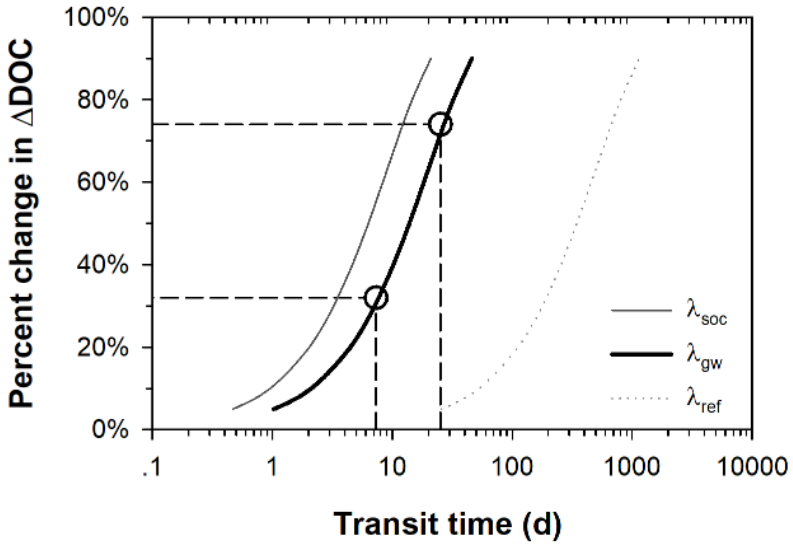

Figure 5. Percent changes in ΔDOC vs MTT (d) shown in log scale. Black line is for the most likely biodegradation rate constant (λ_{gw}) of 0.05 d^{-1} [*Spencer et al.*, 2015]. The different

groundwater MTT is shown as white circles to reflect percent changes in ΔDOC observed at MW in July (32%) and September (74%), respectively. The gray line to the left indicates a constant (λ_{SOC}) of 0.11 d^{-1} at 5°C based on HLGW soil incubation experiment (Table S3). The dotted gray line (λ_{ref}) to the right indicates that MTT estimates using the lowest observed λ of 0.005 d^{-1} based on incubation of Arctic stream water samples [*Balcarczyk et al.*, 2009].

4.3 Hillslopes Act as Hotspots of DOC Processing in Subsurface Environment

Although better constraints on DOC degradation kinetics and repeated monthly sampling from June to December of groundwater would likely result in improved estimates of mean transit time in HLGW, the results nevertheless demonstrate that DOM in permafrost regions of the QTP can be used to shed light on hillslope hydrological process in its headwaters. A long-held view is that aquifer is dominated by water with older ages (> 3 months) compared to riverine systems of much younger water (< 3 months) [*Jasechko et al.*, 2016; *Jasechko et al.*, 2017]. Recent studies suggest a component of groundwater is very young in age [*Gleeson et al.*, 2016], yet unraveling the age distribution is currently challenging with long-term tracer observations [*Luo and Jiao*, 2019; *McDonnell et al.*, 2010]. Though fraught with uncertainties, the estimation above is addressing a challenging problem, and represents the first attempt to quantify hillslope groundwater transit time in the QTP. A global evaluation has shown that the DOC decomposition rate in inland waters ranges from 0.0003 to 9 d^{-1} corresponding to a water retention time of 0.04 day to 42 years [*Catalan et al.*, 2016]. This study supports the notion that hillslopes are hotspots for DOC processing, expanding the coverage of the aforementioned global evaluation to include an important inland water system in QTP.

Existing and newly gained insights on groundwater flow system in HLGW suggest extensive surface water and groundwater interaction, supported by modeling [*Evans et al.*, 2015], isotopic [*Ma et al.*, 2017], hydrochemical [*Li et al.*, 2014; *Li et al.*, 2016] and now DOM quantity and quality data. These studies have identified shallow groundwater sourced primarily from glacier-snow and precipitation [*Chang et al.*, 2018], and flows down gradient above permafrost layer and later above the clay layer (Fig. 1d) [*Evans et al.*, 2015; *Ma et al.*, 2017]. This understanding of groundwater flow together with its extensive interaction with surface water is taken as representative of headwater watersheds with permafrost of alpine hillslopes in the entire QTP.

We put this all together to estimate DOC input and output fluxes to illustrate the extent of DOC loss in HLGW. Considering the significantly lower DOC loss in July than that in September based on differences in ΔDOC, the DOC fluxes were estimated for July and other months, June to December except July. This assumes that September is representative of other months which have lower discharges (Fig. 4), and the input and export of water is mass balanced thus the same. In July, the DOC export is estimated to be 6.8×10^3 kg by multiplying monthly discharge and DOC concentration of outlet stream water (Table 3). The DOC input mass is 8.4×10^3 kg, with the glacier-snow meltwater, precipitation, and soil meltwater contributing 0.3×10^3 kg, 1.7×10^3 kg and 6.4×10^3 kg, respectively (Table 3). Mass balance implies that the "lost" DOC in July is 1.6×10^3 kg (Table 3). Between June to December excluding July, the DOC export is 3.5×10^3 kg by multiplying DOC concentration of outlet stream collected in September with the total discharge of these months. Accordingly, the DOC input is 15.1×10^3 kg with the glacier-snow meltwater, precipitation, and soil melt water contributing 0.6×10^3 kg, 3.1×10^3 kg

and 11.4×10^3 kg, respectively (Table 3). In these five months, "lost" DOC flux amounts to 15.4×10^3 kg (Table 3). Fluxes between January and May are not considered because the discharge is very low and the soil is frozen. The annual DOC input flux is 23.5×10^3 kg, with an annual DOC export flux of 10.3×10^3 kg. The difference between input and export DOC fluxes is taken to represent a "lost" DOC flux of 13.2×10^3 kg within HLGW before transporting into large rivers (Fig. 1c and Table 3). The in-stream loss of such organic carbon accounts for more than half of carbon input mass. In conclusion, the hillslope in headwaters of the Qinghai-Tibetan Plateau act as hotspots for DOM processing, with subsurface environment playing a key role.

Table 3. Input, export and respired DOC fluxes from HLGW.

Input DOC from three endmembers							
End members	DOC (mg/L)	Fraction	July		June-Dec w/o July		Annual flux (10^3 kg/yr)
			Water vol. (10^6 m^3)	DOC mass (10^3 kg)	Water vol. (10^6 m^3)	DOC mass (10^3 kg)	
G	0.5	23%	0.65	0.3	1.16	0.6	
P	1.0	62%	1.74	1.7	3.12	3.1	
S	15.0	15%	0.42	6.4	0.76	11.4	
Input DOC ($x10^3$ kg)				**8.4**		**15.1**	**23.5**
Export DOC at the outlet of HLGW							
Stream at outlet			July		June-Dec w/o July		Annual flux (10^3 kg/yr)
			DOC (mg/L)	Water vol. (10^6 m^3) / DOC mass (10^3 kg)	DOC (mg/L)	Water vol. (10^6 m^3) / DOC mass (10^3 kg)	
Export DOC ($x10^3$ kg)			2.4	2.8 / **6.8**	0.7	5.0 / **3.5**	**10.3**
Loss of DOC during in-stream processing							
			July		June-Dec w/o July		Annual
Loss of DOC (10^3 kg)				**1.6**		**11.6**	**13.2**
% lost DOC				19%		77%	56%

Acknowledgments and Data

We thank field team from CUG, Dr. Qixin Chang, Dr Yalu Hu and Zhao Pan, and staff at the Qilian Station of CAS for their help with the fieldwork and for logistic assistance and quality time; Tom Strekas and Bob Engel of Queens College, CUNY for access to UV-Vis; Junjian Wang of SUSTech for access to TOC-L; Penghui Li and Zhen Tan for discussion on PARAFAC. This study is supported by the National Natural Science Foundation (NSFC Grants No. 41772265, 41831279 and 41228003). Data archiving is underway in Peking University open research data (https://opendata.pku.edu.cn/) repository. All data are compiled and submitted in datasets S1 and S2 of supporting information.

References

Aiken, G. R., R. G. M. Spencer, R. G. Striegl, P. F. Schuster, and P. A. Raymond (2014), Influences of glacier melt and permafrost thaw on the age of dissolved organic carbon in the Yukon River basin, *Global Biogeochemical Cycles*, *28*(5), 525-537.

Ameli, A. A., K. Beven, M. Erlandsson, I. F. Creed, J. J. McDonnell, and K. Bishop (2017), Primary weathering rates, water transit times, and concentration-discharge relations: A theoretical analysis for the critical zone, *Water Resources Research*, *53*(1), 942-960.

Balcarczyk, K. L., J. B. Jones, R. Jaffé, and N. Maie (2009), Stream dissolved organic matter bioavailability and composition in watersheds underlain with discontinuous permafrost, *Biogeochemistry*, *94*(3), 255-270.

Barnes, R. T., D. E. Butman, H. F. Wilson, and P. A. Raymond (2018), Riverine Export of Aged Carbon Driven by Flow Path Depth and Residence Time, *Environmental Science & Technology*, *52*(3), 1028-1035.

Benettin, P., J. W. Kirchner, A. Rinaldo, and G. Botter (2015), Modeling chloride transport using travel time distributions at Plynlimon, Wales, *Water Resources Research*, *51*(5), 3259-3276.

Brogi, S. R., S.-Y. Ha, K. Kim, M. Derrien, Y. K. Lee, and J. Hur (2018), Optical and molecular characterization of dissolved organic matter (DOM) in the Arctic ice core and the underlying seawater (Cambridge Bay, Canada): Implication for increased autochthonous DOM during ice melting, *Science of the Total Environment*, *627*, 802-811.

Catala, T. S., I. Reche, A. Fuentes-Lema, C. Romera-Castillo, E. Ortega-Retuerta, E. Calvo, M. Alvarez, C. Marrase, C. Stedmon, A. A´lvarez-Salgad. (2015), Turnover time of fluorescent dissolved organic matter in the dark global ocean, *Nature Communications*, *6*.

Catalan, N., R. Marce, D. N. Kothawala, and L. J. Tranvik (2016), Organic carbon decomposition rates controlled by water retention time across inland waters, *Nature Geoscience*, *9*(7), 501-+.

Chang, Q., R. Ma, Z. Sun, A. Zhou, Y. Hu, and Y. Liu (2018), Using Isotopic and Geochemical Tracers to Determine the Contribution of Glacier-Snow Meltwater to Streamflow in a Partly Glacierized Alpine-Gorge Catchment in Northeastern Qinghai-Tibet Plateau, *Journal of Geophysical Research-Atmospheres*, *123*(18), 10037-10056.

Cheng, G., and T. Wu (2007), Responses of permafrost to climate change and their environmental significance, Qinghai-Tibet Plateau, *Journal of Geophysical Research*, *112*(F2).

Coble, P. G. (1996), Characterization of marine and terrestrial DOM in seawater using excitation emission matrix spectroscopy, *Marine Chemistry*, *51*(4), 325-346.

Cory, R. M., and D. M. McKnight (2005), Fluorescence Spectroscopy Reveals Ubiquitous Presence of Oxidized and Reduced Quinones in Dissolved Organic Matter, *Environmental Science & Technology*, *39*(21), 8142-8149.

Cory, R. M., C. P. Ward, B. C. Crump, and G. W. Kling (2014), Sunlight controls water column processing of carbon in arctic fresh waters, *Science*, *345*(6199), 925-928.

Cory, R. M., D. M. McKnight, Y.-P. Chin, P. Miller, and C. L. Jaros (2007), Chemical characteristics of fulvic acids from Arctic surface waters: Microbial contributions and photochemical transformations, *Journal of Geophysical Research-Biogeosciences*, *112*(G4).

Drake, T. W., K. P. Wickland, R. G. M. Spencer, D. M. McKnight, and R. G. Striegl (2015), Ancient low–molecular-weight organic acids in permafrost fuel rapid carbon dioxide production upon thaw, *PROCEEDINGS OF THE NATIONAL ACADEMY OF SCIENCES*.

Drake, T. W., F. Guillemette, J. D. Hemingway, J. P. Chanton, D. C. Podgorski, N. S. Zimov, and R. G. M. Spencer (2018), The Ephemeral Signature of Permafrost Carbon in an Arctic Fluvial Network, *Journal of Geophysical Research-Biogeosciences*, *123*(5), 1475-1485.

Evans, S. G., S. Ge, and S. Liang (2015), Analysis of groundwater flow in mountainous, headwater catchments with permafrost, *Water Resources Research*, *51*(12), 9564-9576.

Fellman, J. B., E. Hood, and R. G. M. Spencer (2010), Fluorescence spectroscopy opens new windows into dissolved organic matter dynamics in freshwater ecosystems: A review, *Limnology and Oceanography*, *55*(6), 2452-2462.

Fellman, J. B., D. V. D'Amore, E. Hood, and R. D. Boone (2008), Fluorescence characteristics and biodegradability of dissolved organic matter in forest and wetland soils from coastal temperate watersheds in southeast Alaska, *Biogeochemistry*, *88*(2), 169-184.

Fellman, J. B., E. Hood, R. T. Edwards, and D. V. D'Amore (2009a), Changes in the concentration, biodegradability, and fluorescent properties of dissolved organic matter during stormflows in coastal temperate watersheds, *Journal of Geophysical Research-Biogeosciences*, *114*.

Fellman, J. B., E. Hood, D. V. D'Amore, R. T. Edwards, and D. White (2009b), Seasonal changes in the chemical quality and biodegradability of dissolved organic matter exported from soils to streams in coastal temperate rainforest watersheds, *Biogeochemistry*, *95*(2-3), 277-293.

Feng, X., J. E. Vonk, B. E. van Dongen, O. Gustafsson, I. P. Semiletov, O. V. Dudarev, Z. Wang, D. B. Montlucon, L. Wacker, and T. I. Eglinton (2013), Differential mobilization of terrestrial carbon pools in Eurasian Arctic river basins, *Proceedings of the National Academy of Sciences of the United States of America*, *110*(35), 14168-14173.

Ge, S., J. McKenzie, C. Voss, and Q. Wu (2011), Exchange of groundwater and surface-water mediated by permafrost response to seasonal and long term air temperature variation, Geophysical Research Letters, 38.

Genereux, D. (1998), Quantifying uncertainty in tracer-based hydrograph separations, *Water Resources Research*, *34*(4), 915-919.

Gonçalvesaraujo, R., M. A. Granskog, A. Bracher, K. Azetsuscott, P. A. Dodd, and C. A. Stedmon (2016), Using fluorescent dissolved organic matter to trace and distinguish the origin of Arctic surface waters, *Scientific Reports*, *6*(33978), 33978.

Green, S. A., and N. V. Blough (1994), Optical absorption and fluorescence properties of chromophoric dissolved organic matter in natural waters, *Limnology and Oceanography*, *39*(8), 1903-1916.

Gu, B. H., J. Schmitt, Z. H. Chen, L. Y. Liang, and J. F. McCarthy (1994), ADSORPTION AND DESORPTION OF NATURAL ORGANIC-MATTER ON IRON-OXIDE - MECHANISMS AND MODELS, *Environmental Science & Technology*, *28*(1), 38-46.

Guo, L., and R. W. Macdonald (2006), Source and transport of terrigenous organic matter in the upper Yukon River: Evidence from isotope (delta C-13, Delta C-14, and delta N-15) composition of dissolved, colloidal, and particulate phases, *Global Biogeochemical Cycles*, *20*(2).

Guo, L., C.-L. Ping, and R. W. Macdonald (2007), Mobilization pathways of organic carbon from permafrost to arctic rivers in a changing climate, *Geophysical Research Letters*, *34*(13), n/a-n/a.

Guo, L., Y. Cai, C. Belzile, and R. W. Macdonald (2010), Sources and export fluxes of inorganic and organic carbon and nutrient species from the seasonally ice-covered Yukon River, *Biogeochemistry*, *107*(1-3), 187-206.

Hinkel, K. M., and F. E. Nelson (2003), Spatial and temporal patterns of active layer thickness at Circumpolar Active Layer Monitoring (CALM) sites in northern Alaska, 1995–2000, *Journal of Geophysical Research*, *108*.

Ireson, A. M., G. van der Kamp, G. Ferguson, U. Nachshon, and H. S. Wheater (2013), Hydrogeological processes in seasonally frozen northern latitudes: understanding, gaps and challenges, *Hydrogeology Journal*, *21*(1), 53-66.

Kalbitz, K., and R. Wennrich (1998), Mobilization of heavy metals and arsenic in polluted wetland soils and its dependence on dissolved organic matter, *Science of the Total Environment*, *209*(1), 27-39.

Kawahigashi, M., K. Kaiser, K. Kalbitz, A. Rodionov, and G. Guggenberger (2004), Dissolved organic matter in small streams along a gradient from discontinuous to continuous permafrost, *Global Change Biology*, *10*(9), 1576-1586.

Kling, G. W., G. W. Kipphut, and M. C. Miller (1991), ARCTIC LAKES AND STREAMS AS GAS CONDUITS TO THE ATMOSPHERE - IMPLICATIONS FOR TUNDRA CARBON BUDGETS, *Science*, *251*(4991), 298-301.

Li, C., Chen, P., Kang, S., Yan, F., Tripathee, L., Wu, G., et al. (2018), Fossil Fuel Combustion Emission From South Asia Influences Precipitation Dissolved Organic Carbon Reaching the Remote Tibetan Plateau: Isotopic and Molecular Evidence, *Journal of Geophysical Research-Atmospheres*, *123*(11), 6248-6258.

Li, Z., F. Qi, W. Liu, T. Wang, A. Cheng, Y. Gao, X. Guo,Y. Pan, J. Li, R. Guo (2014), Study on the contribution of cryosphere to runoff in the cold alpine basin: A case study of Hulugou River Basin in the Qilian Mountains, *Global and Planetary Change*, *122*, 345-361.

Li, Z., F. Qi, W. Liu, T. Wang, X. Guo, Z. Li, Y. Gao, Y. Pan, R. Guo, B. Jia, Y. Song and C. Han (2015), The stable isotope evolution in Shiyi glacier system during the ablation period in the north of Tibetan Plateau, China, *Quaternary International*, *380*, 262-271.

Li, Z., F. Qi, Q. J. Wang, Y. Song, H. Li, and Y. Li (2016), The influence from the shrinking cryosphere and strengthening evopotranspiration on hydrologic process in a cold basin, Qilian Mountains, *Global and Planetary Change*, *144*, 119-128.

Luo, X., and J. J. Jiao (2019), Unraveling controlling factors of concentration discharge relationships in a fractured aquifer dominant spring-shed: Evidence from mean transit time and radium reactive transport model, *Journal of Hydrology*, *571*, 528-544.

765 Ma, R., Z. Sun, Y. Hu, Q. Chang, S. Wang, W. Xing, and M. Ge (2017), Hydrological connectivity from glaciers to
766 rivers in the Qinghai-Tibet Plateau: roles of suprapermafrost and subpermafrost groundwater, *Hydrology and*
767 *Earth System Sciences*, *21*(9), 4803-4823.
768 Mann, P. J., T. I. Eglinton, C. P. McIntyre, N. Zimov, A. Davydova, J. E. Vonk, R. M. Holmes, and R. G. M.
769 Spencer (2015), Utilization of ancient permafrost carbon in headwaters of Arctic fluvial networks, *Nature*
770 *Communications*, *6*.
771 Markovich, K. H., A. H. Manning, L. E. Condon, and J. McIntosh (2019), Mountain-Block Recharge: A Review of
772 Current Understanding, *Water Resources Research*.
773 McDonnell, J. J., et al. (2010), How old is streamwater? Open questions in catchment transit time conceptualization,
774 modelling and analysis, *Hydrological Processes*, *24*(12), 1745-1754.
775 McGuire, A. D., L. G. Anderson, T. R. Christensen, S. Dallimore, L. Guo, D. J. Hayes, M. Heimann, T. D.
776 Lorenson, R. W. Macdonald, and N. Roulet (2009), Sensitivity of the carbon cycle in the Arctic to climate
777 change, *Ecological Monographs*, *79*(4), 523-555.
778 McGuire, A. D., et al. (2018), Dependence of the evolution of carbon dynamics in the northern permafrost region on
779 the trajectory of climate change, *Proceedings of the National Academy of Sciences of the United States of*
780 *America*, *115*(15), 3882-3887.
781 McGuire, K. J., and J. J. McDonnell (2010), Hydrological connectivity of hillslopes and streams: Characteristic time
782 scales and nonlinearities, *Water Resources Research*, *46*.
783 McGuire, K. J., J. J. McDonnell, M. Weiler, C. Kendall, B. L. McGlynn, J. M. Welker, and J. Seibert (2005), The
784 role of topography on catchment-scale water residence time, *Water Resources Research*, *41*(5).
785 McKnight, D. M., E. W. Boyer, P. K. Westerhoff, P. T. Doran, T. Kulbe, and D. T. Andersen (2001),
786 Spectrofluorometric characterization of dissolved organic matter for indication of precursor organic material
787 and aromaticity, *Limnology and Oceanography*, *46*(1), 38-48.
788 Mu, C., T. Zhang, Q. Wu, X. Peng, B. Cao, X. Y. Zhang, and G. Cheng (2015), Editorial: Organic carbon pools in
789 permafrost regions on the Qinghai–Xizang (Tibetan) Plateau, *The Cryosphere*, *9*(2), 479-486.
790 Murphy, K. R., C. A. Stedmon, T. D. Waite, and G. M. Ruiz (2008), Distinguishing between terrestrial and
791 autochthonous organic matter sources in marine environments using fluorescence spectroscopy, *Marine*
792 *Chemistry*, *108*(1-2), 40-58.
793 Murphy, K. R., C. A. Stedmon, D. Graeber, and R. Bro (2013), Fluorescence spectroscopy and multi-way
794 techniques. PARAFAC, *Anal. Methods*, *5*(23), 6557-6566.
795 Murphy, K. R., C. A. Stedmon, P. Wenig, and R. Bro (2014), OpenFluor- an online spectral library of auto-
796 fluorescence by organic compounds in the environment, *Anal. Methods*, *6*(3), 658-661.
797 Neff, J. C., J. C. Finlay, S. A. Zimov, S. P. Davydov, J. J. Carrasco, E. A. G. Schuur, and A. I. Davydova (2006),
798 Seasonal changes in the age and structure of dissolved organic carbon in Siberian rivers and streams,
799 *Geophysical Research Letters*, *33*(23).
800 O'Donnell, J. A., G. R. Aiken, E. S. Kane, and J. B. Jones (2010), Source water controls on the character and origin
801 of dissolved organic matter in streams of the Yukon River basin, Alaska, *Journal of Geophysical Research*,
802 *115*(G3).
803 O'Donnell, J. A., G. R. Aiken, M. A. Walvoord, and K. D. Butler (2012), Dissolved organic matter composition of
804 winter flow in the Yukon River basin: Implications of permafrost thaw and increased groundwater discharge,
805 *Global Biogeochemical Cycles*, *26*.
806 Parlanti, E., K. Wörz, L. Geoffroy, and M. Lamotte (2000), Dissolved organic matter fluorescence spectroscopy as a
807 tool to estimate biological activity in a coastal zone submitted to anthropogenic inputs, *Organic Geochemistry*,
808 *31*(12), 1765-1781.
809 Spencer, R. G. M., G. R. Aiken, K. P. Wickland, R. G. Striegl, and P. J. Hernes (2008), Seasonal and spatial
810 variability in dissolved organic matter quantity and composition from the Yukon River basin, Alaska, *Global*
811 *Biogeochemical Cycles*, *22*(4).
812 Spencer, R. G. M., W. Guo, P. A. Raymond, T. Dittmar, E. Hood, J. B. Fellman, and A. Stubbins (2014), Source and
813 biolability of ancient dissolved organic matter in glacier and lake ecosystems on the Tibetan Plateau,
814 *Geochimica et Cosmochimica Acta*, *142*, 64-74.
815 Spencer, R. G. M., P. J. Mann, T. Dittmar, T. I. Eglinton, C. McIntyre, R. M. Holmes, N. Zimov, and A. Stubbins
816 (2015), Detecting the signature of permafrost thaw in Arctic rivers, *Geophysical Research Letters*, *42*(8), 2830-
817 2835.
818 Stedmon, C. A., and R. Bro (2008), Characterizing dissolved organic matter fluorescence with parallel factor
819 analysis: a tutorial, *Limnology and Oceanography-methods*, *6*(11), 572-579.

820 Stedmon, C. A., D. N. Thomas, S. Papadimitriou, M. A. Granskog, and G. S. Dieckmann (2011), Using fluorescence
821 to characterize dissolved organic matter in Antarctic sea ice brines, *Journal of Geophysical Research-*
822 *Biogeosciences*, *116*.
823 Tarnocai, C., J. G. Canadell, E. A. G. Schuur, P. Kuhry, G. Mazhitova, and S. Zimov (2009), Soil organic carbon
824 pools in the northern circumpolar permafrost region, *Global Biogeochemical Cycles*, *23*.
825 Turetsky, M. R., et al. (2020), Carbon release through abrupt permafrost thaw, *Nature Geoscience*, *13*(2), 138-143.
826 Uhlenbrook, S., and S. Hoeg (2003), Quantifying uncertainties in tracer-based hydrograph separations: a case study
827 for two-, three- and five-component hydrograph separations in a mountainous catchment, *Hydrological*
828 *Processes*, *17*(2), 431-453.
829 Vonk, J. E., S. E. Tank, P. J. Mann, R. G. M. Spencer, C. C. Treat, R. G. Striegl, B. W. Abbott, and K. P. Wickland
830 (2015), Biodegradability of dissolved organic carbon in permafrost soils and aquatic systems: a meta-analysis,
831 *Biogeosciences*, *12*(23), 6915-6930.
832 Vonk, J. E., et al. (2013), High biolability of ancient permafrost carbon upon thaw, *Geophysical Research Letters*,
833 *40*(11), 2689-2693.
834 Walvoord, M. A., and R. G. Striegl (2007), Increased groundwater to stream discharge from permafrost thawing in
835 the Yukon River basin: Potential impacts on lateral export of carbon and nitrogen, *Geophysical Research*
836 *Letters*, *34*(12).
837 Wang, B., H. Jin, Q. Li, D. Chen, L. Zhao, Y. Tang, T. Kato, and S. Gu (2017), Diurnal and Seasonal Variations in
838 the Net Ecosystem CO2 Exchange of a Pasture in the Three-River Source Region of the Qinghai-Tibetan
839 Plateau, *PloS one*, *12*(1).
840 Wang, Y., Y. Xu, R. G. M. Spencer, P. Zito, A. Kellerman, D. Podgorski, W. Xiao, D. Wei, H. Rashid, and Y. Yang
841 (2018a), Selective Leaching of Dissolved Organic Matter From Alpine Permafrost Soils on the Qinghai-
842 Tibetan Plateau, Journal of Geophysical Research-Biogeosciences, 123(3), 1005-1016.
843 Wang, Y., R. G. M. Spencer, D. C. Podgorski, A. M. Kellerman, H. Rashid, P. Zito, W. Xiao, D. Wei, Y. Yang, and
844 Y. Xu (2018b), Spatiotemporal transformation of dissolved organic matter along an alpine stream flow path on
845 the Qinghai-Tibet Plateau: importance of source and permafrost degradation, *Biogeosciences*, *15*(21), 6637-
846 6648.
847 Ward, C. P., and R. M. Cory (2015), Chemical composition of dissolved organic matter draining permafrost soils,
848 Geochimica et Cosmochimica Acta, 167, 63-79.
849 Ward, C. P., and R. M. Cory (2016), Complete and Partial Photo-oxidation of Dissolved Organic Matter Draining
850 Permafrost Soils, *Environmental Science & Technology*, *50*(7), 3545-3553.
851 Weishaar, J., G. R. Aiken, B. A. Bergamaschi, M. S. Fram, R. Fujii, and K. Mopper (2003), Evaluation of specific
852 ultraviolet absorbance as an indicator of the chemical composition and reactivity of dissolved organic carbon,
853 *Environmental Science & Technology*, *37*(20), 4702-4708.
854 Wickland, K. P., G. R. Aiken, K. Butler, M. M. Dornblaser, R. G. M. Spencer, and R. G. Striegl (2012),
855 Biodegradability of dissolved organic carbon in the Yukon River and its tributaries: Seasonality and importance
856 of inorganic nitrogen, *Global Biogeochemical Cycles*, *26*(4), n/a-n/a.
857 Wunsch, U. J., J. K. Geuer, O. J. Lechtenfeld, B. P. Koch, K. R. Murphy, and C. A. Stedmon (2018), Quantifying
858 the impact of solid-phase extraction on chromophoric dissolved organic matter composition, *Marine Chemistry*,
859 *207*, 33-41.
860 Xu, J., Q. Zhang, X. Li, X. Ge, C. Xiao, J. Ren, and D. Qin (2013), Dissolved Organic Matter and Inorganic Ions in
861 a Central Himalayan Glacier-Insights into Chemical Composition and Atmospheric Sources, *Environmental*
862 *Science & Technology*, *47*(12), 6181-6188.
863 Yang, M., F. E. Nelson, N. I. Shiklomanov, D. Guo, and G. Wan (2010), Permafrost degradation and its
864 environmental effects on the Tibetan Plateau: A review of recent research, *Earth-Science Reviews*, *103*(1-2),
865 31-44.
866 Yao, Y., C. Zheng, C. Andrews, Y. Zheng, A. Zhang, and J. Liu (2017), What controls the partitioning between
867 baseflow and mountain block recharge in the Qinghai-Tibet Plateau?, *Geophysical Research Letters*, *44*(16),
868 8352-8358.
869 Yi, S., Q. Wang, and W. Sun (2016), Basin mass dynamic changes in China from GRACE based on a multibasin
870 inversion method, *Journal of Geophysical Research-Solid Earth*, *121*(5), 3782-3803.
871 Zhang, G., et al. (2017), Lake volume and groundwater storage variations in Tibetan Plateau's endorheic basin,
872 *Geophysical Research Letters*, *44*(11), 5550-5560.
873